Progress In Electromagnetics Research C, Vol. 172, 38–45, 2026

PIER C

(Received 1 June 2026, Accepted 2 July 2026, Scheduled 29 July 2026)

Multi-Region Efficiency Optimization of Hybrid Electric Vehicle Traction Motors Considering Driving Cycles

Zhijia Jin[1,*], Xinyu Gao[1], Guanghua Li[1], and Kaikai Diao[2]

[1]*School of Automotive Engineering, Suzhou University of Technology, Changshu, China*
[2]*School of Electrical Engineering and Automation, Anhui University, Hefei, China*

ABSTRACT: The conventional optimization of permanent magnet synchronous motors (PMSMs) for hybrid electric vehicles (HEVs) often neglects the dynamic nature of real-world driving cycles, resulting in suboptimal overall energy efficiency. To address this issue, this study proposes a multi-region efficiency optimization strategy that fully integrates actual driving cycles. First, motor operating points were extracted from the WLTC and CLTC standard driving cycles and identified as key operating regions via cluster analysis. A variance-based sensitivity analysis is then employed to quantify the contribution of each rotor parameter, thereby reducing the optimization dimension. The NSGA-III algorithm, coupled with finite element analysis (FEA), performs multi-objective optimization, targeting average efficiency and permanent magnet cost. A new method that comprehensively considers the average efficiency of both the cluster centers and boundaries of the operating points was proposed as an optimization objective. The results show that the optimal candidate improves the average efficiency to 96.77%. Depending on the practical requirements, different candidate points are ultimately selected by balancing efficiency, cost, and driving comfort.

1. INTRODUCTION

Hybrid electric vehicles (HEVs), through the collaborative operation of internal combustion engines and electric motors, can improve fuel efficiency and reduce reliance on fossil energy [1]. Hence, HEVs have served as a critical means of addressing energy shortages. Among them, permanent magnet synchronous motors (PMSMs) have become the predominant type of traction motor in HEVs, owing to their advantages such as high power density and high reliability [2, 3].

Due to the strong nonlinearity and multi-parameter optimization characteristics of PMSMs, their optimization issues have always been a focal point. In recent years, numerous studies have been conducted to enhance the electromagnetic performance of these motors and reduce their manufacturing costs [4–7]. To offer high power density and cost effectiveness, [8] optimized a PMSM by minimizing the mass of active materials via analytical models and particle swarm optimization, resulting in a 44.17% increase in power density. Ref. [9] proposed a multi-region high-efficiency optimization method for PMSMs. The torque-speed region was meshed into grids, and the optimized regions were selected based on the grid energy distribution. The efficiency of each region was improved by optimizing its representative points. To address the rising cost of rare-earth PMSM caused by increasing rare-earth prices, sensitivity analysis, back propagation (BP) neural network surrogate modeling, and genetic algorithm optimization were applied to reduce PM cost under torque and core loss constraints in [10]. Finite element simulations confirmed a 15.59% cost reduction. The aforementioned studies have effectively enhanced the electromagnetic torque of motors or reduced the cost of permanent magnet materials using various optimization methods. However, despite some studies focusing on automotive motors' optimization, most of them are limited to the motor's steady-state or rated operating conditions, failing to fully incorporate the vehicle's actual driving environment. Existing optimizations fail to comprehensively account for the dynamic nature of real-world driving cycles, including acceleration, deceleration, and frequent start-stop events, leaving significant room for improvement in overall energy efficiency.

Optimization that integrates HEV operating conditions or energy management strategies is an effective approach to address the issue. Ref. [11] presented a nested design-based system-level optimization method for PMSMs in HEV, considering the synergies between motor and energy management. The results demonstrate that the optimization strategy can achieve a better overall vehicle performance. In [12], a PMSM with a V-type rotor structure was optimized using OptiSlang and validated in an urban drive cycle over a wide speed range, ensuring practical relevance for real-world EV operation. Additionally, [13] proposed a data-driven methodology that directly links dynamic driving cycles with the statistical distribution of traction motor operating points. The proposed methodology enables an effective trade-off between vehicle performance and driving efficiency while downsizing motor drive components for higher range and lower system cost. Refs. [14] and [15] adopted a similar approach that integrates motor operating points with vehicle driving cycles, thereby making the drive motor more suitable for the corresponding vehicle. In summary, an optimization method that integrates vehicle operating conditions, driving cycles, and energy management strategies can enhance

* Corresponding author: Zhijia Jin (202400006@szut.edu.cn).

comprehensive energy efficiency and applicability of the drive motor under actual driving conditions more effectively.

In addition to the issue of optimization strategies for HEV motors, the efficiency of the motor optimization process itself is also critical. Sensitivity analysis, surrogate models, and intelligent optimization algorithms are commonly used to improve the efficiency of motor optimization [16, 17]. Ref. [18] proposed a surrogate modeling method using machine learning algorithms to capture the complex relationship between structural parameters and output objectives. Subsequently, an improved genetic algorithm was adopted to obtain the optimal combination of motor parameters. Similarly, a new surrogate modeling and optimal design method for PMSM based on deep forest and Bayesian optimization algorithm was proposed in [19]. The feasibility of a scheme combining surrogate models with intelligent optimization algorithms was verified for motor structure optimization. However, owing to the large number of motor parameters and significant differences in their impacts on electromagnetic performance, a sensitivity analysis is required to screen the variables to be optimized before optimization process. Commonly used sensitivity analysis methods include the Pearson correlation coefficient method [18], analysis of variance [19], and Morris method [20], all of which have been applied to motor optimization problems.

Currently, the dynamic nature of real-world driving cycles remains largely overlooked in existing motor optimization studies, leaving considerable room for improving the overall energy efficiency under actual vehicle operation. Moreover, the reasonable selection of motor operating points according to specific driving conditions and the determination of the final optimization strategy based on the differences among numerous operating points should be considered. Therefore, this study proposes a multi-region efficiency optimization strategy for PMSM rotors using sensitivity analysis and intelligent optimization algorithms, aiming to improve the motor's overall efficiency under real-world operating conditions and thereby enhance vehicle fuel economy. The main contributions of this study are as follows:

1) A multi-region efficiency optimization strategy for PMSM used in HEVs was proposed. The motor operating points to be optimized were obtained from real HEV driving cycles. The motor operating points to be optimized were divided into regions using cluster analysis, and a new method for calculating the average efficiency of the cluster center and boundary was employed.
2) Analysis of variance was employed to screen the rotor variables, and a co-simulation strategy combining finite element analysis (FEA) of the operating points with the NSGA-III algorithm was adopted during the optimization process, thereby improving the optimization efficiency.

The remainder of this paper is structured as follows. In Section 2, the architecture of the HEV and topology of the PMSM are introduced. Section 3 illustrates the main multi-region efficiency optimization, including an analysis of PMSM operating points, sensitivity analysis, and the complete optimization process. The optimization results and discussions are presented in Section 4, followed by the conclusion in Section 5.

2. THE TOPOLOGY AND OPERATING ENVIRONMENT OF THE MOTOR

The structure of the motor to be optimized is illustrated in Fig. 1. It is a three-phase, eight-pole, 48-slot interior PMSM. The initial dimensional parameters of the motor are listed in Table 1. The PMSM operates in a coaxial parallel HEV, which additionally comprises an automated manual transmission (AMT), engine, and traction battery, among other components. The output power from the engine is transmitted through the AMT and coupled with the motor power before being delivered to the wheels. The entire architecture of the HEV is shown in Fig. 2. In the HEV, the PMSM primarily operates under vehicle operating modes, such as low-speed start-up, combining power output with the engine under high power demand, and regenerative braking mode.

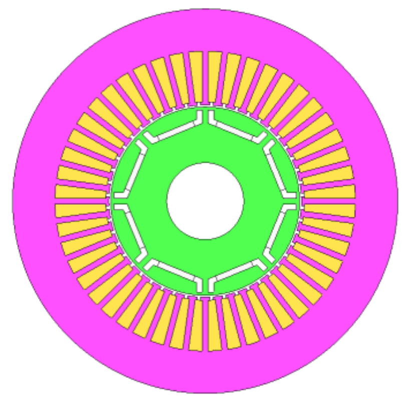

FIGURE 1. Structure of the PMSM.

TABLE 1. Initial dimension parameters of the motor.

Symbol	Parameters	Values
D_{mag}	Magnet inner radius/mm	38
D_{slit}	Flux bridge thickness/mm	1.5
SW	Flux barrier width/mm	3
$Slit$	Interpole flux barrier width/mm	3
T_{mag}	Magnet thickness/mm	3
W_{mag}	Magnet width/mm	19.5
g	Air gap length/mm	1.2
D_o	Stator Outer Diameter/mm	200
D_i	Rotor Inner Diameter/mm	100
D_{sh}	Shaft Diameter	40
b_{01}	Slot Opening Width	1.8
h_{01}	Slot Opening Height	1.6
h_2	Slot Depth	22
b_t	Tooth Width	3
L	Stack Length	150

Based on the above HEV architecture and PMSM structure, the following section presents the proposed multi-region efficiency optimization strategy.

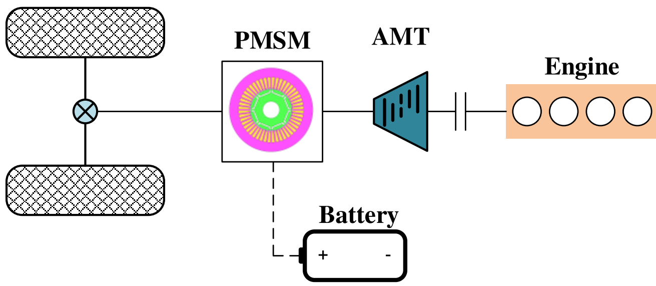

FIGURE 2. Architecture of the HEV.

3. MULTI-REGION EFFICIENCY OPTIMIZATION

The operation of the motor used in HEVs is influenced by the vehicle driving cycle, and the motor operating point is divided into different regions owing to the influence of vehicle control strategies. Therefore, an efficiency optimization strategy tailored to different work areas was proposed.

3.1. Analysis of PMSM Operating Points

Figure 3 presents two commonly used test cycles for passenger cars: WLTC and CLTC. These two cycles cover various operating patterns of passenger vehicles worldwide, including urban, suburban, and high-speed driving conditions, respectively. In this study, the HEV architecture depicted in Fig. 2 was operated under selected driving cycles, followed by an analysis of the motor operating points.

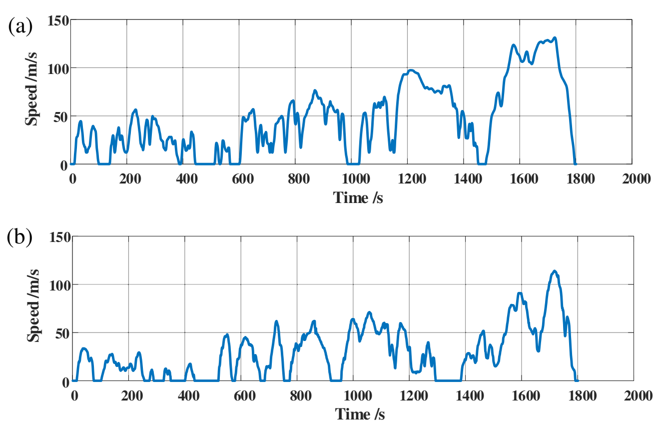

FIGURE 3. Driving cycles of the HEV. (a) WLTC and (b) CLTC.

Figure 4 shows the motor operating points under the two test conditions. As illustrated in the figure, all motor operating points are categorized into five distinct clusters via cluster analysis, with the cluster centers denoted by star symbols labeled C1 to C5. Specifically, the blue cluster (C1) represents a high-frequency operating region corresponding to low-speed urban cruising conditions. The red cluster (C2) involves high-speed and high-torque operations, corresponding to extreme-speed driving conditions. The yellow cluster (C3) features relatively low speed but moderate torque, representing low-speed starting and congested traffic conditions for HEVs. The purple cluster (C4) characterizes mid-speed aggressive acceleration and overtaking maneuvers. The green cluster (C5) corresponds to high-speed cruising conditions in suburban areas. The frequencies of clusters C1–C5 are 4.44%, 26.20%, 37.52%, 27.62%, and 4.23%, respectively.

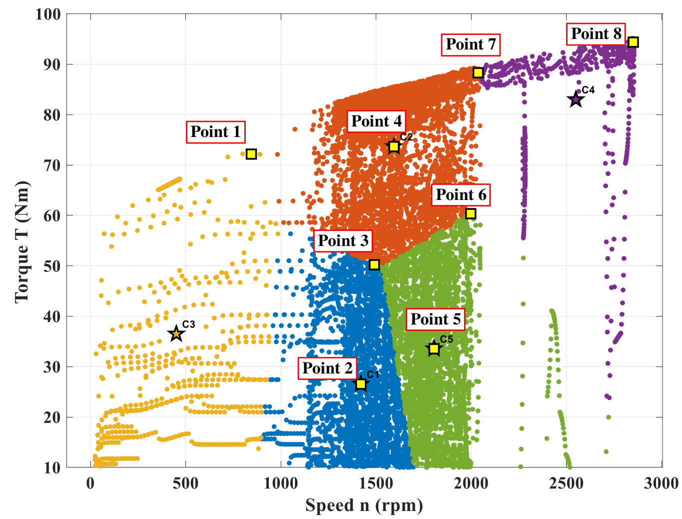

FIGURE 4. Operating points of the PMSM.

In addition, based on the results of the cluster analysis and the division of boundaries in this study, the final operating points to be optimized were selected, marked as squares in the figure, and the specific data points are provided in Table 2. Points 2, 4, and 5 are the cluster centers in the high-frequency operation ranges, which ensure the optimal efficiency of the motor within its commonly used ranges. The other operating points are the clustering boundaries. The boundary points make the motor performance distribution more uniform across the entire torque-speed plane, eliminating the issue of uncovered blank areas between the clustering centers.

TABLE 2. Operating points to be optimized.

Point	Speed/rpm	Torque/Nm
1	844	72.2
2	1420	26.5
3	1490	50.2
4	1593	73.7
5	1804	33.5
6	1997	60.3
7	2036	88.3
8	2851	94.4

3.2. Sensitivity Analysis

In a motor optimization design, there are often many parameters to optimize. If global optimization is performed directly on all the parameters, the computational cost becomes extremely high. Therefore, it is particularly important to conduct a sensitivity analysis before a detailed optimization. In this study, analysis of variance was adopted to perform a sensitivity analysis on the rotor parameters of the electric motor, and the formula is as follows:

$$S(x_i) = \frac{V(E(f/x_i))}{V(f)} \tag{1}$$

where f is the optimization objective, $E(f/x_i)$ the average value of f when x_i is constant, $V(E(f/x_i))$ the variance of $E(f/x_i)$, and $V(f)$ the variance of f.

In the analysis of variance, a variable with a percentage contribution (PC) exceeding 50% is generally considered to play a dominant role in influencing the optimization objective. A PC between 20% and 50% indicates that the variable is an important factor, whereas a PC between 5% and 20% suggests it is a secondary factor. If the PC is less than 5%, the variable has a weak effect on the optimization objective and can be excluded from the optimization. Fig. 5 shows the results of the analysis of variance. It is evident that the torque and cost of T_{mag}, as well as the ripple of g, have PC values exceeding 50%. Therefore, T_{mag} and g are set as the dominant factors in this study. Most of the other variables have PC values ranging from 5% to 20%, and are thus set as secondary factors. It is proven that all the aforementioned seven parameters need to be optimized.

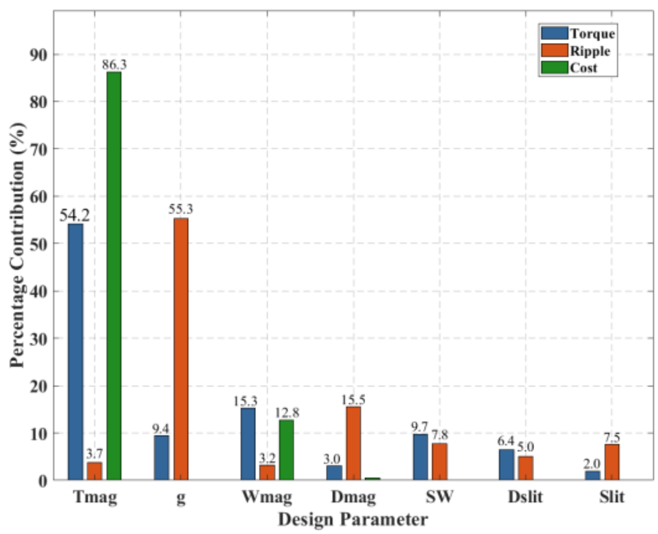

FIGURE 5. The results of analysis of variance.

3.3. Optimization Strategy

Figure 6 shows the optimization flowchart in this study, including initialization, optimization analysis, and optimization process steps.

In addition to the motor cost, this study directly considers the operating point efficiency under the selected test-driving cycles. Therefore, the optimization objectives and constraints can be expressed as follows:

$$\min : \begin{cases} -\mathit{eff} = -\mathit{eff}_{\max}(x_1, x_2, \ldots, x_n) \\ \text{Cost} = P_c(x_1, x_2, \ldots, x_n) \end{cases} \tag{2}$$

$$\text{s.t.} \begin{cases} P_c(x_1, x_2, \ldots, x_n) \le P_{\text{need}} \\ T_{\max}(x_1, x_2, \ldots, x_n) \ge T_{\text{need}} \\ R_p(x_1, x_2, \ldots, x_n) \le R_{\text{need}} \end{cases} \tag{3}$$

where $T_{\max}$ is the maximum torque, P_c the cost, R_p the torque ripple, x_i the parameters to be optimized, and *eff* the average efficiency of each point to be optimized, which can be generally expressed as

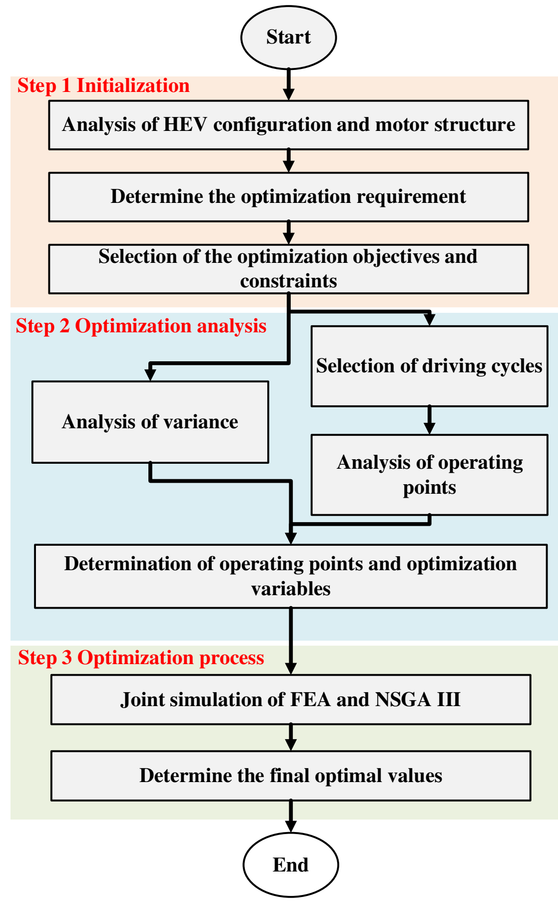

FIGURE 6. Flowchart of the optimization process.

$$\mathit{eff} = \frac{1}{n}\sum_{i=1}^{n} \mathit{eff}_i \tag{4}$$

where n is the number of sampling points. In this study, it should be noted that torque ripple is imposed as a hard constraint rather than a third optimization objective. For HEV traction motors, average efficiency and magnet cost are the primary design drivers that directly determine fuel economy and manufacturing expense, while torque ripple mainly affects noise, vibration, and harshness (NVH) performance. Once the ripple level falls within an acceptable range, further reduction will only bring minor benefits.

However, owing to differences in frequency among clusters, as well as the varying roles played by the cluster center and boundary points, the efficiency weight of each working point should vary. Therefore, a novel method for calculating the average efficiency is proposed in this study as follows:

$$\mathit{eff} = \sum_{i=1}^{n_c} \omega_{ci} \cdot \mathit{eff}_{ci} + \sum_{i=1}^{n_b} \omega_{bi} \cdot \mathit{eff}_{bi} \tag{5}$$

where n_c and n_b are the number of sampling points for the cluster center and boundary, respectively, and ω_c and ω_b are weights, which can be calculated as follows:

$$\omega_c = \alpha \cdot f_k$$
$$\omega_b = f_k \cdot \frac{1-\alpha}{n_k} \tag{6}$$

where α is the center priority coefficient, with a value of 0.75 in this study, f_k the frequency of the k-th cluster, and n_k the number of boundary points in the k-th cluster.

After determining optimization objectives, analyzing parameter sensitivity, and selecting operating points, the optimization process can proceed. NSGA-III is recognized as a highly efficient multi-objective evolutionary algorithm that is extensively employed in industrial settings to tackle multi-objective optimization problems [21, 22]. Consequently, this algorithm was adopted in the current study to optimize the PMSM. The NSGA-III algorithm proceeds through a sequence of key steps: population initialization, generation of offspring via crossover and mutation, merging of parent and offspring populations, non-dominated sorting, environmental selection, and formation of the next generation population. During the iteration process of NSGA-III, the calculation for each population involves using FEA software to perform torque, ripple, and efficiency calculations on the selected motor operating points. Finally, the optimal rotor structure is selected based on the optimization results.

4. RESULTS AND ANALYSIS

Before optimization, the ranges of rotor parameters to be optimized are given in Table 3. The ranges are defined based on typical motor design references and manufacturing tolerances, and further refined by FEA parametric sweeps.

TABLE 3. Range of rotor parameters to be optimized.

Symbol	Ranges/mm
D_{mag}	36–40
D_{slit}	1–2
SW	2–4
$Slit$	2–4
T_{mag}	2–4
W_{mag}	17–22
g	0.8–1.5

Figure 7 shows the Pareto frontiers of the optimization. This Pareto frontier illustrates the non-dominated relationship between motor cost and average efficiency at operating points. The color of the points on the frontier represents the average torque of the points to be optimized, which is used to assess whether the torque satisfies the constraint. The maximum average efficiency is 96.77%, the minimum is 96.07%, and the maximum amplitude variation is 0.7%; the maximum area of the permanent magnet is 87.08 mm^2; and the minimum is 34.1 mm^2, yielding a ratio of more than 2.5 : 1.

Considering the distribution of the Pareto frontier, four candidate points are ultimately selected as the optimal results for

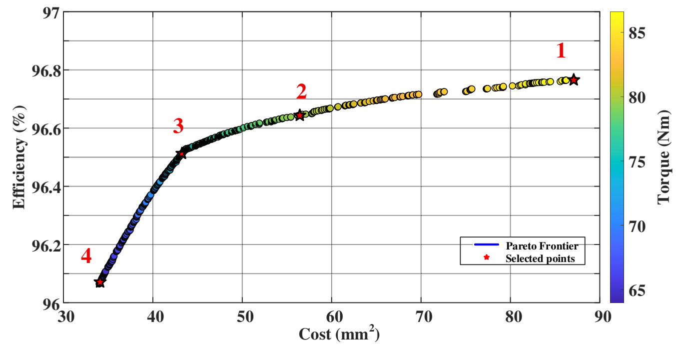

FIGURE 7. Pareto frontier of the optimization.

further consideration, and these points are marked with red stars in Fig. 7. The specific parameters of these four candidate points are listed in Table 4. Fig. 8 presents the complete efficiency MAP diagrams for the four candidate points. Candidate 1 exhibits both the highest efficiency and largest output torque, with a peak efficiency of approximately 97.7%, whereas the peak efficiencies of the other three candidate points do not exceed 97.5%. This feature also corresponds to dimensions of the permanent magnets at each candidate point.

TABLE 4. Results of the candidate points.

Point	g (mm)	T_{mag} (mm)	W_{mag} (mm)	SW (mm)	D_{mag} (mm)	D_{slit} (mm)	$Slit$ (mm)
1	0.80	3.96	21.99	3.91	39.78	1.00	3.99
2	0.80	2.57	21.96	3.91	39.83	1.00	3.99
3	0.80	2.00	21.63	3.91	39.83	1.00	3.99
4	0.80	2.00	17.05	3.91	39.83	1.00	3.99

To further screen the final optimization results, this study incorporates each motor candidate point into the HEV model to analyze the corresponding driving performance. The parameters of the HEV model are listed in Table 5. CLTC is selected as the test-driving cycle, with a simulation duration of 1800 s. In addition, all candidate points adopted the same energy management strategy and control parameters during the simulations.

TABLE 5. Parameters of the vehicle.

Parameters	Value
Vehicle mass/kg	1400
Frontal area/m^2	1.75
Tire radius/m	0.287
Rolling resistance coefficient	0.008
Aerodynamic drag coefficient	0.3
Peak power of engine/kW	62
Battery capacity/Ah	120

Figures 9 and 10 show the battery state of charge (SOC) and fuel consumption curves under different candidate points, respectively. The results indicate that the trends of the vehicle SOC and fuel consumption curves remain largely consistent across the four different candidate motors. This can be attributed to the fact that, under fixed energy management con-

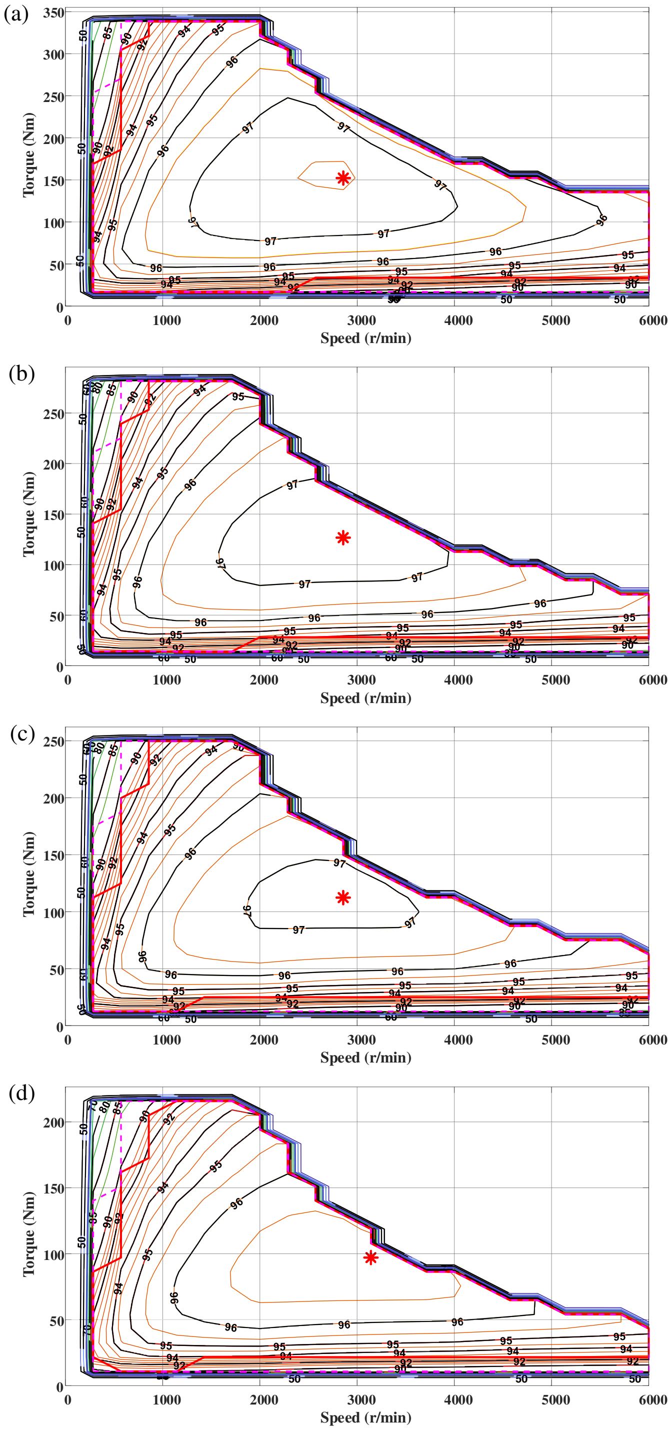

FIGURE 8. Efficiency MAPs of the candidates. (a) Candidate 1, (b) candidate 2, (c) candidate 3, and (d) candidate 4.

trol parameters, as long as the motor output torque meets the demand, the motor operating points remain nearly unchanged. Consequently, only the differences in motor efficiency affect electricity and fuel consumption. After optimization, the differences among the four candidate points in terms of motor operating points are relatively small. Consequently, in a single test cycle, the differences in HEV performance corresponding to each candidate point are not very pronounced; nevertheless, a clear pattern of variation still exists. Candidate 1 achieves

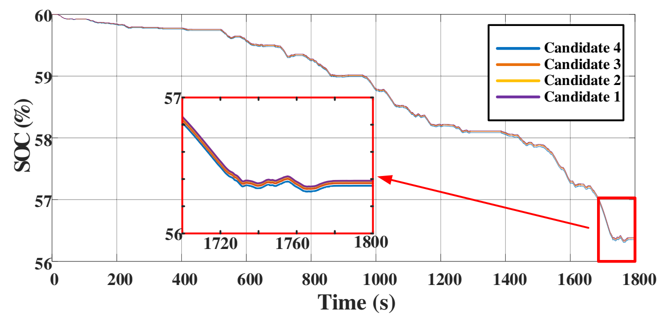

FIGURE 9. Battery SOC curves under different candidate points.

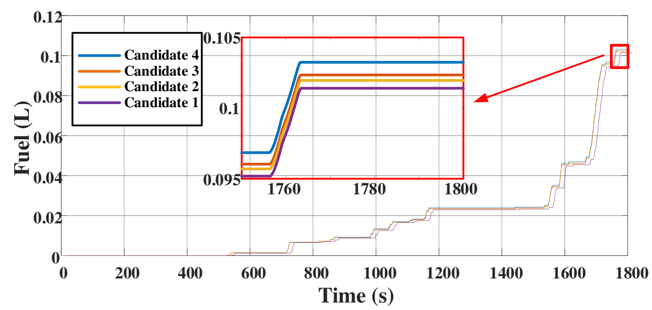

FIGURE 10. Fuel consumption curves under different candidate points.

TABLE 6. HEV performance under different candidate points.

Candidate	SOC/%	Fuel/L
1	56.3875	0.1014
2	56.3844	0.1020
3	56.3701	0.1023
4	56.3506	0.1032

the lowest fuel consumption after simulation, at only 0.1014 L, while retaining the highest SOC of 56.3875%. As the permanent magnet area decreases, the fuel consumption of the candidate points gradually increases, and the remaining SOC gradually decreases. The maximum differences in fuel consumption and SOC are 0.0018 L and 0.0369%, respectively. The detailed data are presented in Table 6.

Figure 11 presents the torque waveforms of the four candidate motors at several selected operating points, aiding in the final selection of candidate points. It can be noted that the torque ripple comparison in Fig. 11 focuses on Points 2–5, because they belong to the highest-frequency operating clusters. Points 2, 4, and 5 are the cluster centers in high-frequency operation ranges, and Point 3 is located on the boundary of three high-frequency clustering regions and serves as a representative transition operating point. Table 7 presents the calculated torque ripple values.

If only the efficiency goal is considered, candidate 1, with the highest average efficiency, most remaining SOC, and lowest fuel consumption, may be the optimal solution. However, candidate 4 offers the smallest PM area, and hence, the lowest cost. Its fuel consumption increases slightly compared with those of candidates 2 and 3. More importantly, it achieves the

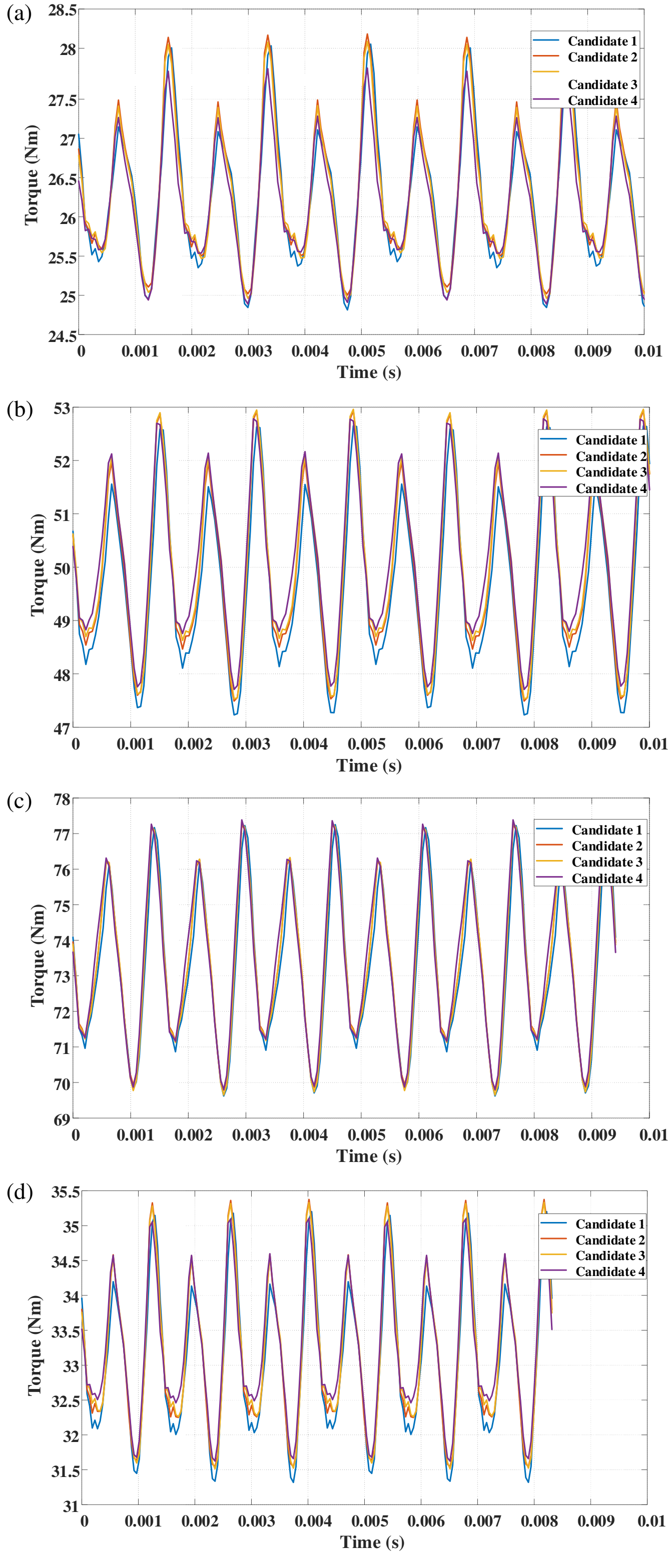

FIGURE 11. Torque waveform at operating points. (a) Point 2, (b) Point 3, (c) Point 4, and (d) Point 5.

best average torque ripple of 10.46%, significantly improving the NVH of the HEV. Candidates 2 and 3 provide marginal efficiency gains at much higher cost and worse ripple. Considering both the cost and driving comfort, candidate 4 can also be selected. In summary, if the focus is solely on efficiency, candidate 1 is an optimal solution; however, if cost and driving comfort are considered, candidate 4 is preferable.

TABLE 7. Torque ripple at operating points.

Candidate	Point 2	Point 3	Point 4	Point 5
1	12.33%	10.91%	10.42%	11.74%
2	12.08%	10.91%	10.18%	11.55%
3	11.91%	10.85%	10.45%	11.51%
4	10.92%	10.12%	10.32%	10.48%

To verify the numerical reliability of the FEA model, a mesh sensitivity analysis was conducted based on candidate 4. Fig. 12 shows the variation of the average torque with respect to the mesh density coefficient. As the mesh density increases, the calculated torque rapidly converges to a stable value of approximately 49.87 Nm, with a fluctuation less than 2% across the entire valid range of mesh densities. This confirms that the FEA solutions are mesh-independent.

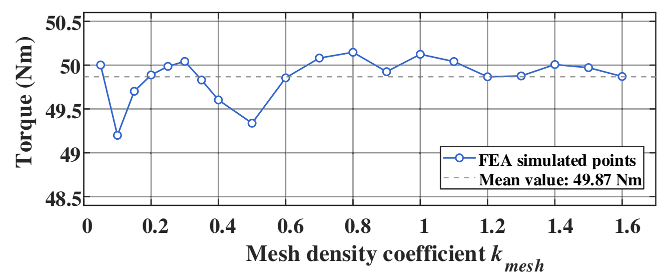

FIGURE 12. Mesh sensitivity analysis.

5. CONCLUSION

In this study, a multi-region efficiency optimization strategy for PMSM was proposed. The main contributions of this study are as follows.

(1) The operating points of the PMSM under real driving cycles were used for motor optimization. Cluster analysis was employed to identify the characteristic operating points corresponding to the different operating modes. The cluster centers and mode boundary points were selected for efficiency optimization, and a novel efficiency-weight assignment scheme was proposed to account for the differences between the boundary points and cluster centers.

(2) Through a sensitivity analysis based on an analysis of variance, the rotor parameters to be optimized were identified. An optimization strategy combining NSGA-III with FEA was then adopted, thereby improving the optimization efficiency of PMSM.

(3) The Pareto frontier of the average efficiency and cost was obtained. Candidate points were selected and simulated in conjunction with the HEV model. Finally, the optimal solution was determined based on the optimized efficiency, HEV driving performance, cost, and driving comfort. When only the efficiency objective is consid-

ered, candidate 1 is preferred; when cost and comfort are considered, candidate 4 is preferred.

It should be noted that the current study relies exclusively on FEA without physical prototype testing. Future work will focus on manufacturing the optimal prototype and conducting experimental measurements.

ACKNOWLEDGEMENT

This work was supported by the Natural Science Foundation of the Jiangsu Higher Education Institutions of China (Grant No. 1020241096).

REFERENCES

[1] Chiver, O., I. R. Sugar, and L. Neamt, "Study on the selection of electric motor/engine on the performance of hybrid vehicles," *Energies*, Vol. 17, No. 14, 3529, 2024.

[2] Liu, Y., Z. Wei, K. Ma, and Z. Zhang, "Improved thermal management and analysis for high-power heat pipe cooled FSCW PMSM for HEV auxiliary power unit application," *IEEE Transactions on Energy Conversion*, Vol. 39, No. 2, 1154–1167, 2024.

[3] Eduku, S., J. Sekyi-Ansah, M. O. Alhassan, and E. N. Odonkor, "Design optimization and comparative performance analysis of a novel five-phase fault-tolerant spoke-type flux-switching permanent magnet motor for EV/HEV applications," *Journal of Electrical Engineering & Technology*, Vol. 20, No. 3, 1541–1556, 2025.

[4] El Hajji, T., S. Hlioui, F. Louf, M. Gabsi, G. Mermaz-Rollet, and M. Belhadi, "Optimal design of high-speed electric machines for electric vehicles: A case study of 100 kW V-shaped interior PMSM," *Machines*, Vol. 11, No. 1, 57, 2023.

[5] Liu, F., X. Wang, and H. Wei, "Electromagnetic performance analysis, prediction, and multiobjective optimization for U-type IPMSM," *IEEE Transactions on Industrial Electronics*, Vol. 71, No. 9, 10 322–10 334, 2024.

[6] Meddour, A. R., N. Rizoug, P. Leserf, C. Vagg, R. Burke, and C. Larouci, "Optimization of the lifetime and cost of a PMSM in an electric vehicle drive train," *Energies*, Vol. 16, No. 13, 5200, 2023.

[7] Yuan, B., H. Li, X. Xiang, and H. Zhou, "Energy efficiency optimization design for cycle position servo PMSM based on operating energy consumption model," *IEEE Open Journal of the Industrial Electronics Society*, Vol. 6, 591–602, 2025.

[8] Kolsi, H., N. B. Hadj, M. Chaieb, and R. Neji, "Design of permanent magnet synchronous motor by means of power density optimization for e-vehicle applications," *International Review on Modelling & Simulations*, Vol. 15, No. 3, 203, 2022.

[9] Zhu, X., M. Jiang, Z. Xiang, L. Xu, Y. Chen, and L. Quan, "Design and optimization of a multi-region high-efficiency permanent magnet motor with enhanced energy efficiency," *IEEE Transactions on Energy Conversion*, Vol. 40, No. 3, 2169–2178, 2025.

[10] Wang, B., G. Liu, Z. Xu, and F. Zhang, "Cost optimization method for less-rare-earth permanent magnet synchronous motor based on surrogate model," in *2024 27th International Conference on Electrical Machines and Systems (ICEMS)*, 1808–1813, Fukuoka, Japan, 2024.

[11] Sun, X., Z. Dong, Z. Jin, G. Lei, and X. Tian, "System-level energy management optimization of power-split hybrid electric vehicle based on nested design," *IEEE Transactions on Industrial Electronics*, Vol. 71, No. 9, 10 987–10 997, 2024.

[12] Sardar, M. U., D. Manfeng, U. Saleem, M. Hassan, and M. K. Nawaz, "State-of-the-art design optimization of an IPM synchronous motor for electric vehicle applications," in *2022 International Conference on Emerging Trends in Electrical, Control, and Telecommunication Engineering (ETECTE)*, 1–6, Lahore, Pakistan, 2022.

[13] Mohammadi, H., S. Saini, R. Nasirizarandi, and A. Balamurali, "Drive cycle-based design optimization of traction motor drives for battery electric vehicles using data-driven approaches," Tech. Rep., SAE, 2024.

[14] Lee, G.-h. and Y.-m. You, "Efficiency optimization of the main operating points of an ev traction motor," *Applied Sciences*, Vol. 15, No. 1, 368, 2025.

[15] Mahmouditabar, F., E. F. Farahani, V. Pickert, and M. C. Kulan, "Multi-physics LCA-based design optimization of an interior permanent magnet motor for EVs," *Energies*, Vol. 18, No. 23, 6167, 2025.

[16] Zhang, Y., L. Fei, C.-K. Chui, C.-B. Chng, S. Zhao, and J. Li, "Machine learning surrogate model optimized by improved sparrow search algorithm for multi-objective optimization of permanent magnet synchronous motor direct-drive pump," *IEEE Transactions on Vehicular Technology*, Vol. 73, No. 9, 12 773–12 786, 2024.

[17] Zhu, Z., X. Li, Y. Lin, H. Wu, J. Chen, N. Zhang, T. Wu, B. Lin, and S. Wang, "Multi-objective optimization design of high-power permanent magnet synchronous motor based on surrogate model," *Sustainability*, Vol. 18, No. 3, 1705, 2026.

[18] Liu, L., Y. Guo, W. Yin, G. Lei, X. Sun, and J. Zhu, "Efficient design optimization of pmsm drive systems using improved equivalent-circuit-based loss minimization control," *IEEE Transactions on Industrial Electronics*, Vol. 72, No. 4, 3280–3291, 2025.

[19] Xu, N., X. Sun, and C. H. T. Lee, "Hierarchical multiobjective optimization of spoke-type axial-flux pmsms using transfer learning and improved grey wolf algorithm," *IEEE Transactions on Industrial Electronics*, Vol. 73, No. 5, 6780–6791, 2026.

[20] Braband, M., M. Scherer, and H. Voos, "Global sensitivity analysis of economic model predictive longitudinal motion control of a battery electric vehicle," *Electronics*, Vol. 11, No. 10, 1574, 2022.

[21] Jiang, X., J. Niu, J. Xu, T. Zhang, W. Zhou, Q. Jiang, J. Xu, and K. Ma, "Design and optimization of a lightweight five-phase permanent magnet fault-tolerant motor based on improved NSGA-III," *IEEE Transactions on Transportation Electrification*, Vol. 12, No. 2, 2899–2909, 2026.

[22] Hernandez, C., J. Lara, M. A. Arjona, F. J. Martinez, J. E. Moron, R. Escarela-Perez, and J. Sykulski, "Electromagnetic optimal design of a PMSG considering three objectives and using NSGA-III," *IEEE Transactions on Magnetics*, Vol. 58, No. 9, 1–4, 2022.